



# A spatio-spectral polarization analysis of 1 $\mu\text{m}$ -pumped bulk supercontinuum in a cubic crystal (YAG)

Aradhana Choudhuri<sup>1,2</sup> · Gourab Chatterjee<sup>1</sup> · Jiaan Zheng<sup>2</sup> · Ingmar Hartl<sup>2</sup> · Axel Ruehl<sup>3,4</sup> · R. J. Dwayne Miller<sup>1</sup>

Received: 16 October 2017 / Accepted: 30 April 2018  
© The Author(s) 2018

## Abstract

We present the first systematic study of the spatio-spectral polarization properties of a supercontinuum generated in a cubic crystal, yttrium–aluminum garnet (YAG), including a full spectral analysis of the white light core and surrounding ring structure. We observe no depolarization of the supercontinuum, and no spatial dependence of polarization ratios for any wavelength. We discuss the discrepancy of YAG's polarization behavior in the context of well-established results in literature reporting self-induced depolarization in other cubic crystals.

The growing demand for coherent radiation beyond the spectral coverage of laser gain materials can currently only be met via parametric processes (DFGs and OPAs) seeded by highly nonlinear processes like hollow-core fiber and bulk supercontinuum (SC) generation [1–5]. Seeding a parametric process directly via SC can greatly reduce the complexity and number of stages required in an amplification setup. However, pumping the SC process with femtosecond and picosecond pulses in the 10–100  $\mu\text{J}$  range raises questions regarding nonlinear effects that may have a significant impact on the efficiency of the polarization-sensitive parametric process to be seeded. Given the induced polarization rotation of intense pump pulses in various SC-candidate nonlinear materials, and the wavelength-dependent depolarization of bulk SC [13], a significant portion of seed energy may be lost if the desired wavelengths lie in the high depolarization spectral region of the SC output.

Many of the bulk materials commonly used for ultra-broadband SC generation, including  $\text{CaF}_2$ ,  $\text{BaF}_2$  and YAG,

exhibit a cubic crystal structure. Studies have reported cross-polarized wave generation and polarization rotation of the intense pump pulse during propagation in cubic crystals, leading to a depolarization of the SC output [10, 11, 13]. This effect has been demonstrated in various crystals, including  $\text{CaF}_2$  [13, 17–19]. In contrast, SC generated in YAG shows little or no depolarization [20]. This creates a puzzling discrepancy between theoretical predictions [17, 18] for polarization rotation in cubic crystals, versus the experimental findings of polarization maintenance in YAG.

The spectral output of SC in bulk crystals is an ultra-broadband pulse with frequencies centered around the pumping wavelength and a spatial structure consisting of a central white light (WL) core surrounded by colored rings (the Conical Emission, CE) [6–8]. A significant portion of the spectral energy of the SC output lies in the frequencies found in the CE [8]—the presence of the same frequencies in the WL core, especially the far-from-pump anti-Stokes peak, has been identified as the axial portion of the CE [8, 9], implying a good phase relationship between identical frequency components in the CE and the WL. The spectral output in the WL is asymmetric, with higher energies in the anti-Stokes wing and an exponential drop-off of energy far from the pump [7]. In the case of polarization-sensitive processes like OPAs and DFGs seeded with specific wavelengths in the low energy-density region of the SC output, careful management of depolarization and beamline losses is required to efficiently generate the desired output [1, 2, 4]. In addition, if the CE has a well-behaved polarization state, it opens the possibility of utilizing the CE energies in addition to the WL core itself.

✉ Gourab Chatterjee  
gourab.chatterjee@mpsd.mpg.de

<sup>1</sup> Max Planck Institute for the Structure and Dynamics of Matter, Luruper Chaussee 149, 22761 Hamburg, Germany

<sup>2</sup> Deutsches Elektronen-Synchrotron (DESY), Notkestrasse 80, 22761 Hamburg, Germany

<sup>3</sup> Present Address: QUEST-Leibniz-Research School, Institute of Quantum Optics, Leibniz University Hannover, Welfengarten 1, 30167 Hanover, Germany

<sup>4</sup> Laser Zentrum Hannover e.V., Hollerithallee 8, 30419 Hanover, Germany

Third-order processes (including space–time focusing, self-steepening, plasma generation, third harmonic generation, etc.) are by far the largest contributors to spectral generation in the bulk SCG process. The  $\chi^{(3)}$  tensor of the bulk SC material governs the dynamics and interplay of these processes. The abrupt “explosion-like” self-steepening and pulse-splitting at the onset of SCG is accompanied by degenerate four-wave mixing (due to momentum conservation) that results in the creation of the conical emission [31]. The nonlinearly induced polarization rotation of the pump pulse at these peak intensities arises out of the momentum terms during the self-steepening process [16–18].

Bucharov et al. proposed that different wavelengths of light are produced at different positions along the propagation path of the intense pump pulse [13]. As per this interpretation, we posit that if the rotated portion of the pump generates portions of the SC spectra, the CE should be depolarized. Further, we expect that a polarization modulation/rotation of the intense input pulse should be imprinted upon the polarization properties of the ringed structure of the SC output. Should SC generated in YAG exhibit depolarization due to YAG’s crystal structure and the anisotropy of its  $\chi^{(3)}$  tensor, the proposed mechanism of action for depolarization [13, 18] would be most clearly evident in a spatio-spectral depolarization analysis of the CE as a radial position-based modulation of the polarization ratio.

In this paper, we study the polarization properties of the entire spatio-spectral structure of the output of a bulk SC process in YAG, and present the first spatio-spectral study of SC generation in a cubic crystal, including its ring structure. Our work also highlights the possibility of utilizing the CE as well as the WL of the SC to seed subsequent parametric amplification stages.

While there is a lot of debate regarding the exact mechanisms giving rise to SC characteristics [7], the general consensus is that the process is heavily reliant upon the third-order susceptibility tensor  $\chi^{(3)}$ . Input (pump) field intensity affects many critical nonlinearities via the mediation of the  $\chi^{(3)}$  tensor. In addition, cross-polarized wave generation of intense incident light in cubic crystals is dependent upon the orientation of the crystal planes with respect to the pulse propagation direction [11, 12].

For our experiments, pump pulse energy and intensity were chosen to maximize the probability of observing depolarization and cross-polarized wave generation, without pushing the SC output into an unstable or multi-filament regime. Pump peak power and intensity fall within the range covered by similar studies in the literature, e.g., [13–17]. As the growth direction of the YAG crystal with respect to its crystallographic plane orientation can be a factor contributing to crystal anisotropy, we chose a [1,1,1] cut, as this is the only cut where the thermally induced birefringence is independent of the original growth direction [21]. Furthermore,

the [1,1,1] cut has theoretically a high anisotropy of the  $\chi^{(3)}$  tensor under various orientations of incident pump polarization [10]. Should this anisotropy be a factor for SC generation, choosing such a crystal cut would maximize the depolarization dependence on incident pump polarization angle.

A schematic of the optical setup is shown in Fig. 1. The 180 fs, 10 kHz, 1032 nm output of a ytterbium diode-pumped solid-state laser system (Pharos, light conversion), linearly polarized at 600:1, was attenuated to 10  $\mu$ J and focused to a Gaussian waist diameter of approximately 30  $\mu$ m into the 5 mm long YAG crystal using a 100 mm fused-silica (FS) lens. An iris before the focusing optics was used to optimize the numerical aperture of the beam for SC generation. The pump laser has a pulse-to-pulse stability of <0.5% (rms) and power stability of <0.5% (rms) over 24 h. Environmental vibrations produce a beam-pointing jitter of approximately  $\pm 1$  mm over 24 h at the input lens. The YAG sample was rotated about the  $z$ -axis during setup w.r.t. optimizing conversion efficiency and polarization for the fundamental and second harmonic wavelength of the pump. No difference was noted in polarization or conversion efficiency based on crystal rotation.

The highly divergent and broadband SC output beam was roughly collimated with a 2”-diameter, 150-mm focal-length FS lens. A 1-mm pinhole on a motorized translation stage allowed sampling of the beam at various transverse positions ( $x$ -axis). Due to the ultra-broadband nature of the SC output, a thin-film polarizer scheme (required for a full analysis of the Stokes vectors of the SC output) could not be used. Instead, a Glan-Taylor polarizer on a rotation stage was mounted behind the pinhole to quantify the linear component of the polarization state sufficient to determine the degree of polarization rotation. A broadband, multimode fiber (non-polarization maintaining, as only the total flux transmitted by the fiber was relevant) was used to sample the output of the polarizer and deliver the light to a spectrometer. The presence of widely different divergence angles and the inability to focus all of them equally upon the fiber-tip resulted in a modulation structure of the fiber-sampled spectra, which disappeared when the full output was focused on the fiber tip, or collected using an integrating sphere. The setup was also sensitive to input beam-pointing spatial instabilities over the course of the measurement period.

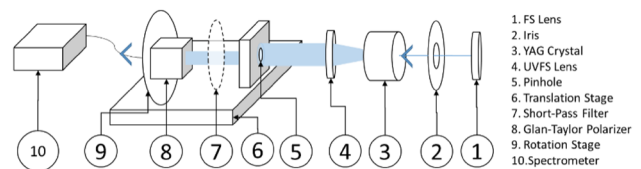


Fig. 1 Schematic of the experimental setup

Maximum depolarization during SC generation is often reported on the anti-Stokes side of the SC output [17], and there is an exponential dropoff of spectral energy density on the red side leading to small changes in polarization being lost in background noise. Therefore, only the anti-Stokes portion of the SC output was used for this study.

Data taken over the course of a day using an integrating sphere were compared to the integrated spectral intensity  $I_\lambda$  derived from the pinhole-sampled data using:

$$I_\lambda = \frac{\sum_x I_{\lambda,x} \pi(x^2 - (x-d)^2)}{A} \tag{1}$$

where  $I_{\lambda,x}$  is the spectral intensity recorded at radius  $x$  from the center of the beam with a pinhole diameter  $d$  and  $A$  is the total sampled area of the output. This comparison is shown in Fig. 2. Both datasets were normalized using the pump intensity measured for each technique (input pulse without SC crystal) at 1 μm, just below the short-pass filter (Thorlabs FESH1000) cutoff. The pinhole-derived data fall within  $1\sigma$  of the mean of the integrating sphere data and shows good general agreement in terms of spectral shape, highlighting the validity of our spatial sampling technique. Due to the presence of the filter used to attenuate the pump wavelength, spectra above 1 μm are not used for intensity-comparison

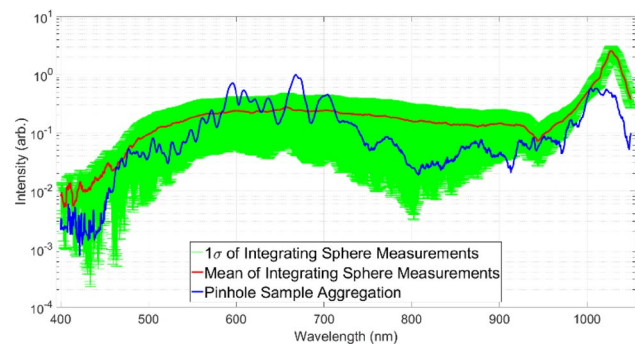
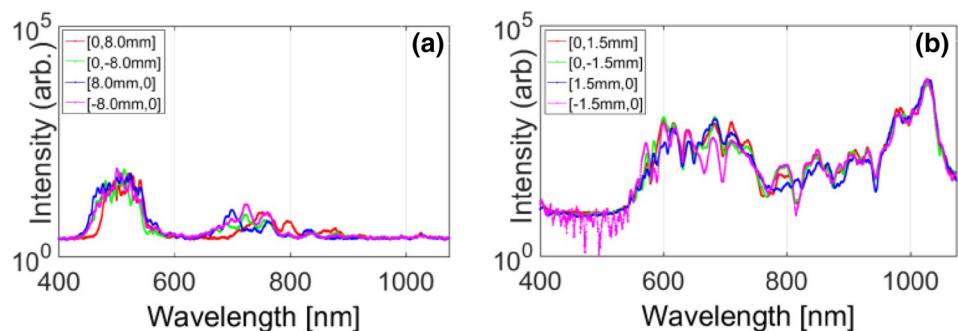


**Fig. 2** Comparison of SC output spectra—integrated values extrapolated from pinhole-sampled spectra (blue), and integrating sphere values over 1 day—mean (red),  $1\sigma$  extent (green)

**Fig. 3** Optical spectrum at four sampling positions with a radial distance of **a**  $r=8$  mm and **b**  $r=1.5$  mm, measured by the pin-hole sampling method described in the text



to other wavelengths. Additionally, the pinhole method imposes a tight tolerance, i.e., it rejects residual non-collimated portions of the pump wavelength which are collected and sampled by the integrating sphere method, leading to a discrepancy between the two methods at the intense pump wavelength.

The SC output was scanned in the transverse direction in 0.5-mm intervals over a beam radius of 10 mm (2-mm WL core radius, 10-mm maximal CE radius). At each spatial position, the polarizer was rotated by  $360^\circ$ , in  $5^\circ$  increments, and spectral data were recorded. Spatial symmetry of the output was verified via spectra taken at radially symmetric positions around the center of the beam (Fig. 3). There is good agreement in spectral shape for identical radii. Working with a radially symmetric beam allows us to reduce the spatial analysis of the polarization to a single dimension.

Figure 4a shows the spectral dependence of the polarization contrast, which follows the spectral energy density,

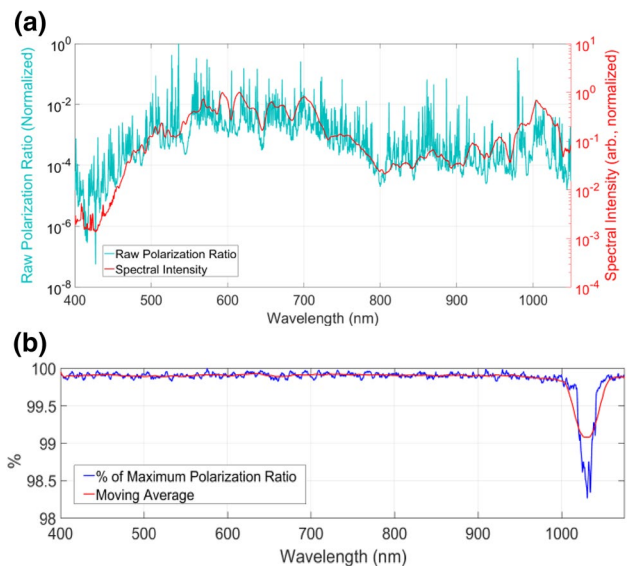


**Fig. 4** **a** Spectral intensity (integrated over all sampling positions) vs wavelength (red) and polarization ratio vs wavelength (blue). **b** Percentage of maximum polarization ratio vs wavelength (integrated over all sampling positions) (blue) and moving average (red)

suggesting a wavelength dependency of the polarization ratio, as reported in [13]. This is merely a measurement artifact due to the different power levels available at each wavelength. For example, if 10  $\mu\text{J}$  are available near pump wavelengths with a noise-floor of 100 nJ, it leads to a maximum possible polarization ratio of 100:1, whereas if only 1  $\mu\text{J}$  is available at 800 nm, it leads to a maximum possible polarization ratio of 10:1. The maximum polarization ratio is the decisive parameter and can be calculated as:

$$\rho_{\max,\lambda} = \sum_x \rho_{\max,\lambda,x} = \left( \frac{\sum_x I_{\lambda,x,\parallel}}{\sum_x I_{\lambda,x,\perp}} \right) \times 100\%, \quad (2)$$

where  $I_{\lambda,x,\parallel}$  and  $I_{\lambda,x,\perp}$  are the intensities for a wavelength  $\lambda$  measured in the plane parallel and perpendicular, respectively, to the linear polarization of the incident pulse at a specific sampling location  $x$ . When plotting the  $\rho_{\max,\lambda}$  trend as done in Fig. 4b, we find that the SC output is highly polarized, with a moving average of 99.8%. The intense pump pulse itself does show a slight degree of depolarization, but the polarization-preservation in the SC output confirms the findings of Silva et al., namely that the SC generated in YAG is not depolarized, and follows the polarization of the pump pulse [20]. As the maximum possible polarization ratio developed here is dependent upon the noise threshold, Fig. 4b. shows that there is a constant polarization ratio through the spectrum only up to the limitation imposed by the measured noise.

The SC output exhibits multiple rings of the same color but different divergence angles, and it is assumed that regardless of the relative retardation of red frequency generation during a single cycle, each distinct spatial ring of a specific wavelength is created in a different focusing/defocusing cycle of the SC process. This guarantees multiple points of origin for each color along the evolution of the pump pulse in the nonlinear medium and allows evaluation of the impact of spatial pump / SC overlap on the polarization state of the SC output. The maximum polarization ratio with respect to the transverse position is shown in Fig. 5 for selected wavelengths. As expected from Fig. 4b, a high degree of

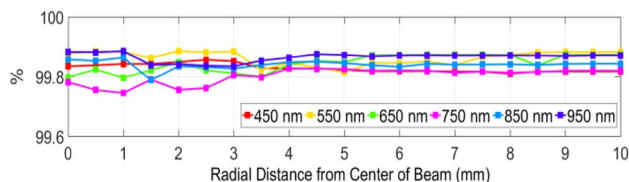


**Fig. 5** Percentage of maximum polarization ratio of SC output in respect to the radial position for various wavelengths, measured by the pin-hole sampling method described in the text

polarization (similar to the spatially integrated measurement shown in Fig. 4b) is present at any transverse position at any wavelength, despite the drastically different spectral contents at different transverse positions (see Fig. 3). This highlights that under the experimental conditions used here, the spatial overlap between the pump beam and the SC does not lead to a polarization rotation via cross-phase modulation or any other nonlinear effect as suggested in Ref. [13].

Our experimental results are puzzling, given the anisotropy of the  $\chi^{(3)}$  tensor in YAG [23], which has a form identical to that of  $\text{CaF}_2$ , where a strong wavelength-dependent depolarization has been observed in previous studies, for example, in [13]. The nonlinear index is, at its root, a function of the hyperpolarizability of the electron distribution forming the bonds in crystals [24]. The hyperpolarizability of oxygen in YAG varies up to a factor of 10, that of fluorine in  $\text{CaF}_2$  varies by a factor of 7 [24], whereas the value of the nonlinear indices for  $\text{CaF}_2$  and YAG are also very similar,  $1.9 \times 10^{-16} \text{ cm}^2/\text{W}$  [20] and  $2.9 \times 10^{-16} \text{ cm}^2/\text{W}$  [15], respectively;  $\text{CaF}_2$  has an even lower nonlinear index than YAG. This should lead to an experimentally observable depolarization of the SC output in YAG that is greater than, or at least comparable, to  $\text{CaF}_2$ . Yet the SC-generated broadband portion of the output pulse in YAG demonstrates a distinct lack of depolarization—increasing input energies in the hopes of seeing depolarization results in multifilamentation and a destruction of the spatial structure of the output we wish to study. In the operating regime, the minor polarization rotation of the intense pump, consistent with theory [17], is not imprinted onto the SC output. We propose that the marginally depolarized portion of the pump is not sufficient to contribute to the nonlinear processes that create the SC output.

It should be noted that it is difficult to compare the true extent of depolarization of SC output vs. intense pump pulse polarization rotation. Studies that focus on wavelength-based depolarization effects of SC generation in  $\text{CaF}_2$  use the raw polarization ratio and not a function of the maximum-possible polarization ratio as a metric.

Nagura et al. generated SC in  $\text{CaF}_2$  and various other media far in excess of  $P_{\text{cr}}$  in the materials, and found depolarization of the SC output only in the cubic crystals  $\text{CaF}_2$  and  $\text{LiF}$ , concluding that the SC is polarized in the direction of the incident light in an isotropic material, but not cubic materials [18]. Kartzaev et al. generated SC in  $\text{CaF}_2$  and reported a crystal plane orientation dependent, self-induced polarization rotation of the pump, with a direct influence on the polarization properties of the anti-Stokes wing of the SC output spectra [15]. Johnson et al. [30] discovered polarization modulation in the SC output of  $\text{CaF}_2$  pumped with linearly-polarized light vs. a very high degree of polarization preservation for the circularly-polarized pump case (which would mask any induced polarization rotation). As cross-polarized wave generation in cubic crystals is well



established, there is no intrinsic reason that the mechanisms behind self-induced polarization of intense pulses should be readily apparent in  $\text{CaF}_2$  but not in YAG.

Kumar et al. studied SC depolarization as a function of pump intensity [16] and demonstrated the role of crystallographic orientation—even in a non-centrosymmetric crystal-like KDP, the authors found that if the crystal is oriented correctly, SC output preserves the input-polarization state. This directly supports the findings of this paper, i.e. that YAG SC output is well polarized. Therefore, we look to origins beyond the anisotropy of the  $\chi^{(3)}$  tensor to explain the discrepancy between YAG and  $\text{CaF}_2$  SC output.

$\text{CaF}_2$  exhibits an intrinsic birefringence [27], and strong UV absorption at the blue edge of the SC output leading to damage [29].  $\text{CaF}_2$  is easily damaged, and requires continual rotation of the  $\text{CaF}_2$  plate for SC applications [30]. The crystal also has a tendency to grow in the  $\langle 110 \rangle$  direction [28] with implications of the crystal-plane orientation rotating and introducing defects throughout the length of the rod as growth proceeds, which may account for the polarization modulation of SC output reported in [30] for a rotated  $[001]$   $\text{CaF}_2$  sample. Depolarization due to damage caused by the intense incident pulses has been reported, not only in the case of  $\text{CaF}_2$ , but also for other nonlinear media. Inhomogeneities in electron density of the induced plasma would invariably arise in a damaged bulk crystal. The polarization state of the generated SC can also differ from pump even in isotropic amorphous media due to inhomogeneity in the electron density, and subsequent scattering as reported in Ref. [16]. Furthermore, Dharmadhikari et al. reported a 100-fold polarization degradation at the onset of multi-photon ionization occurring well below the damage threshold [14]. All of the above factors may contribute significantly to observed depolarization (to an extent not expected to arise solely from  $\chi^{(3)}$ -based polarization-rotation of intense pump pulses) of SC generated in  $\text{CaF}_2$ .

In light of the above factors, we believe that the crystallographic quality of nonlinear media used for SC generation must be taken into account, and the degree of depolarization of SC output demonstrated in fluoride crystals  $\text{CaF}_2$ ,  $\text{BaF}_2$  and  $\text{LiF}$  has origins beyond the anisotropy of the  $\chi^{(3)}$  tensor. The absence of depolarization in  $\text{CaF}_2$  is also suggested in an application in literature: For example, Huber et al. detail a  $\text{CaF}_2$  SC-seeded BBO OPA (a polarization sensitive process) without the use of the customary polarization-correction optics—by stringently controlling crystal quality, the authors used the SC directly for OPA seeding [32], which leads us to infer that the SC output was well polarized. This leads us to conclude that to study the SC process, specifically nonlinear pump polarization rotation and other  $\chi^{(3)}$ -based effects that only become apparent at higher intensities, using  $\text{CaF}_2$  and related crystals (where crystallographic plane orientation variations may exist) would cloud the origin of the effect

being studied. We suggest that YAG is a more representative crystal—to the best of our knowledge, there are no reports of YAG plates used for SC requiring rotation to prevent damage or any of the other issues (intrinsic birefringence, crystal-plane rotation during growth) of  $\text{CaF}_2$ . Structural studies of YAG show excellent crystal hardness, with low creep and stress-induced birefringence [26]. Consistent with the theory on polarization-rotation in cubic crystals, YAG shows polarization rotation of the pump, but this small fraction of the intense input pump does not contribute to SC generation, and the superior crystal quality of YAG allows us to observe the intrinsic polarization of the SC output itself, which arises from the un-rotated portion of the pump. As an extension to this work, similar analysis on the Stokes-side SC output might give interesting results directly applicable to MIR OPA/OPCPA studies.

In summary, we present the first full spatio-spectral polarization analysis of the output of a bulk SC generation process in YAG and confirm the polarization-preservation nature across the entire spatial and spectral profile by introducing the maximum polarizability as the decisive quantity. We discuss the disparity between the well-known polarization preservation in YAG and the depolarization in other cubic crystals such as  $\text{CaF}_2$ . Given the highly polarized nature of the SC output beam across the entire spectral and spatial domains (even in the presence of some minor depolarization of the intense pump), we conclude that while studies of self-induced polarization rotation during highly nonlinear processes such as SC generation are fundamentally correct, the extent of depolarization of SC output studied in crystals like  $\text{CaF}_2$  is highly influenced by crystallographic quality and bulk damage, and is not intrinsic to SC generation in cubic nonlinear crystals.

**Acknowledgements** The authors thank Christian Kraenkel (Zentrum für Lasermaterialien - Kristalle (ZLM-K) am Leibniz-Institut für Kristallzüchtung (IKZ)) for the helpful discussions on the crystallographic quality of  $\text{CaF}_2$  and YAG.

**Open Access** This article is distributed under the terms of the Creative Commons Attribution 4.0 International License (<http://creativecommons.org/licenses/by/4.0/>), which permits unrestricted use, distribution, and reproduction in any medium, provided you give appropriate credit to the original author(s) and the source, provide a link to the Creative Commons license, and indicate if changes were made.

## References

1. A. Dubietis, G. Tamosauskas, R. Suminas, V. Jukna, A. Couairon, *Lith. J. Phys.* **57**, 113 (2017)
2. A. Dubietis, G. Jonušauskas, A. Piskarskas, *Opt. Commun.* **88**, 437 (1992)
3. C. Manzoni, G. Cerullo, *J. Opt.* **18**, 103501 (2016)

4. H. Fattahi, H.G. Barros, M. Gorjan, T. Nubbemeyer, B. Alsaif, C.Y. Teisset, M. Schultze, S. Prinz, M. Haefner, M. Ueffing, A. Alismail, L. Vámos, A. Schwarz, O. Pronin, J. Brons, X.T. Geng, G. Arisholm, M. Ciappina, V.S. Yakovlev, D. Kim, A.M. Azzeer, N. Karpowicz, D. Sutter, Z. Major, T. Metzger, F. Krausz, *Optica* **1**, 45 (2014)
5. Y. Deng, A. Schwarz, H. Fattahi, M. Ueffing, X. Gu, M. Ossian-der, T. Metzger, V. Pervak, H. Ishizuki, T. Taira, T. Kobayashi, G. Marcus, F. Krausz, R. Kienberger, N. Karpowicz, *Opt. Lett.* **37**, 4973 (2012)
6. A.-L. Calendron, H. Çankaya, G. Cirmi, F.X. Kärtner, *Opt. Express* **23**, 13866 (2015)
7. A. Couairon, A. Mysyrowicz, *Phys. Rep.* **441**, 47 (2007)
8. A. Jarnac, M. Durand, A. Houard, Y. Liu, B. Prade, M. Richardson, A. Mysyrowicz, *Phys. Rev. A* **89**, 023844 (2014)
9. M. Durand, K. Lim, V. Jukna, E. McKee, M. Baudelet, A. Houard, M. Richardson, A. Mysyrowicz, A. Couairon, *Phys. Rev. A* **87**, 043820 (2013)
10. S. Kourtev, N. Minkovski, L. Canova, A. Jullien, O. Albert, S.M. Saltiel, *J. Opt. Soc. Am. B* **26**, 1269 (2009)
11. N. Minkovski, S. Kourtev, L. Canova, A. Jullien, O. Albert, R. Lopez-Martens, *Opt. Lett.* **36**, 301 (2011)
12. N. Minkovski, S. M Saltiel, G. I Petrov, O. Albert, J. Etchepare, *Opt. Lett.* **27**(22), 2025 (2002)
13. I. Buchvarov, A. Trifonov, T. Fiebig, *Opt. Lett.* **32**, 1539 (2007)
14. A.K. Dharmadhikari, F.A. Rajgara, D. Mathur, *Opt. Lett.* **31**, 2184 (2006)
15. V. Kartazhev, R.R. Alfano, *Opt. Commun.* **281**, 463 (2008)
16. R.S.S. Kumar, K.L.N. Deepak, D.N. Rao, *Phys. Rev. A* **78**, 043818 (2008)
17. K. Midorikawa, H. Kawano, A. Suda, C. Nagura, M. Obara, *Appl. Phys. Lett.* **80**, 923 (2002)
18. C. Nagura, A. Suda, H. Kawano, M. Obara, K. Midorikawa, *Appl. Opt.* **41**, 3735 (2002)
19. J. Yu, H. Jiang, J. Wen, H. Yang, Q. Gong, *Opt. Express* **18**, 12581 (2010)
20. F. Silva, D.R. Austin, A. Thai, M. Baudisch, M. Hemmer, D. Faccio, A. Couairon, J. Biegert, *Nat. Commun.* **3**, 807 (2012)
21. W. Koechner, D.K. Rice, *J. Opt. Soc. Am.* **61**, 758 (1971)
22. I. Shoji, T. Taira, *Appl. Phys. Lett.* **80**, 3048 (2002)
23. P.N. Butcher, D. Cotter, *The Elements of Nonlinear Optics*, 1st edn. Cambridge University Press, Cambridge (1990)
24. R. Adair, L.L. Chase, S.A. Payne, *Phys. Rev. B* **39**, 3337 (1989)
25. R.S.S. Kumar, K.L.N. Deepak, D. Narayana, Rao, *Opt. Lett.* **33**, 1198 (2008)
26. Y. Nie, M. Zhang, Y. Liu, Y. Zhao, *J. Alloys Compd.* **657**, 184 (2016)
27. J. Burnett, Z. Levine, E. Shirley, *Phys. Rev. B* **64**, 241102 (2001)
28. N. Senguttuvan, M. Aoshima, K. Sumiya, H. Ishibashi, *J. Cryst. Growth* **280**, 462 (2005)
29. A. Brodeur, S.L. Chin, *Phys. Rev. Lett.* **80**, 4406 (1998)
30. P.J.M. Johnson, V.I. Prokhorov, R.J.D. Miller, *Opt. Express* **17**, 21488 (2009)
31. D. Faccio, M.A. Porras, A. Dubietis, F. Bragheri, A. Couairon, P. Di Trapani, *Phys. Rev. Lett.* **96**, 193901 (2006)
32. R. Huber, H. Satzger, W. Zinth, J. Wachtveitl, *Opt. Commun.* **194**, 443 (2001)